Northern Hemisphere Storm Tracks in Present Day and Last Glacial Maximum Climate Simulations: A Comparison of the European PMIP Models*

M. Kageyama, P. J. Valdes, G. Ramstein, C. Hewitt, U. Wyputta

HAL Id: hal-02931782
https://hal.science/hal-02931782

Submitted on 8 Feb 2021

Northern Hemisphere Storm Tracks in Present Day and Last Glacial Maximum Climate Simulations: A Comparison of the European PMIP Models*

M. KAGEYAMA

*Department of Meteorology, University of Reading, Reading, United Kingdom, and
Laboratoire des Sciences du Climat et de l'Environnement, UMR, CEA–CNRS, Gif-sur-Yvette, France*

P. J. VALDES

Department of Meteorology, University of Reading, Reading, United Kingdom

G. RAMSTEIN

Laboratoire des Sciences du Climat et de l'Environnement, UMR, CEA–CNRS, Gif-sur-Yvette, France

C. HEWITT

*Hadley Centre for Climate Prediction and Research, United Kingdom Meteorological Office,
Bracknell, Berkshire, United Kingdom*

U. WYPUTTA

University of Bremen, Bremen, Germany

(Manuscript received 12 September 1997, in final form 20 February 1998)

ABSTRACT

Extratropical weather systems are an essential feature of the midlatitude climate and global circulation. At the last glacial maximum (LGM), the formation of regions of high transient activity, referred to as ''storm tracks,'' is strongly affected by the presence of large ice sheets over northern America and Scandinavia and by differences in sea surface temperature (SST) distributions. In the framework of the Palaeoclimate Modelling Intercomparison Project, simulations of the LGM climate have been run with a wide range of atmospheric general circulation models (AGCMs) using the same set of boundary conditions, allowing a valuable comparison between simulations of a climate very different from the present one.

In this study, the authors focus on the storm track representation in the models and its relationship with the surface temperatures, the mean flow, and the precipitation. Storm tracks are described using transient eddy diagnostics such as mean sea level pressure variance and three-dimensional **E** vectors, computed from daily output. It is found that the general response to the changes in boundary conditions from present day to LGM is consistent for all models: they nearly all give an eastward shift for both storm tracks, with a larger shift for the Atlantic one. This is intrinsically linked to changes in stationary waves, which is also studied using the **E** vector diagnostic. Differences between the models reside in the value of the shift of the storm tracks and the change in their amplitude, which the authors analyze in terms of differences in resolution and parameterizations in the models. The sensitivity of the storm tracks to the sea surface temperatures and sea-ice extent are also examined by comparing the differences between prescribed and computed SST simulations. All in all, it is the eastern part of the storm tracks that is found to be most model-dependent, which relates to differences in the simulated climates over America's west coast and Europe, and has to be taken into account when analyzing GCM climate simulations.

1. Introduction

The midlatitude winter climate is characterized by the frequent occurence of perturbations, alternance of depressions and anticyclones, which play a major role in transferring energy from the equator to the poles. The fronts associated with these perturbations are largely responsible for the precipitation at these latitudes. The

regions of high day-to-day variability (e.g., in mean sea level pressure or in geopotential height), hereafter referred to as ''storm tracks,'' have been extensively studied for the present day climate in observational analyses [see for instance Blackmon (1976), Blackmon et al. (1977), Blackmon et al. (1984), Wallace et al. (1988), Lim and Wallace (1991)], as well as theoretical analyses (Simmons and Hoskins 1980; Hoskins and Valdes 1990; Thorncroft et al. 1993). The perturbations explaining the high-variability characteristic of the storm tracks are recognized as manifestations of the baroclinic instability typical of the mean flow at midlatitudes (Charney 1947; Eady 1949). For the present day climate in the Northern Hemisphere there are two regions of high baroclinicity, situated over the eastern coasts of Asia and America. This is where the meridional gradients of surface temperatures are the strongest, due to the contrasts between the continents and the oceans, and where the upper-level jet streams reach their maxima. These regions see the development of perturbations whose growth is also favored by the diabatic heating and moisture supply provided by the oceans (Hoskins and Valdes 1990). Hence the characteristics of the storm tracks depend on 1) the position of the continents in the surrounding oceans, 2) their orography, which modifies the mean flow, and 3) the surface temperature distribution, which is not independent from points one and two above.

Since atmospheric general circulation models (AGCMs) are able to simulate the present day storm tracks fairly well (see for instance Hall et al. 1996a), it is important, in a climate change perspective, to assess their ability to represent storm-track development under different conditions. These can be provided by palaeoclimate studies. The last glacial maximum (LGM) (21 000 yr ago) is especially interesting because it is relatively well documented and very different from the present climate at the mid- and high latitudes that are of interest for the storm tracks. Indeed ice sheets covered not only Antarctica and Greenland as today, but also northern America (Laurentide ice sheet, maximum about 2.5 km high) and Scandinavia (Fennoscandian ice sheet, maximum about 1.5 km high), leading to a sea level decrease of the order of a 100 m (Peltier 1994). Also, the temperatures of the extratropical oceans were much colder, leading to more extensive sea ice than at present [see for example the conclusions from the Climate Long-Range Investigation Mapping and Prediction (CLIMAP 1981) project]. Analyzing the storm tracks in AGCM simulations can help our understanding of the climates as described by palaeoindicators because they provide a link between the surface temperature and precipitation that can be inferred through this data. In the LGM case, it can also help us to understand how the ice sheets were maintained, since these are ''fed'' by precipitation of which the storms are an important source (Hall et al. 1996b).

General studies of the last glacial maximum climate have been carried out using AGCMs. Kutzbach and Guetter (1986) performed perpetual January runs and found an increase and a southward shift of the storm tracks, accompanied by an increase of precipitation over the Pacific, but not over the Atlantic. Rind (1987) also performed perpetual January runs and found an increase of baroclinicity and eddy kinetic energy for the mid-latitude storm tracks along with less rainfall over the western United States and Europe, but more over the eastern United States. Hall et al. (1996a,b) ran simulations of the full seasonal cycles and found consistent eastward shifts of regions of high baroclinicity, 850-hPa eddy temperature fluxes and 250-hPa eddy kinetic energy in winter. They also observed that the dramatic increase in the low-level eddy activity, particularly over the Atlantic, did not propagate to higher levels. Results from these studies therefore appear to be quite dependent on the model used. In our study, we present simulations from nine models and find that the eastward shift of the storm tracks noticed by Hall et al. (1996a,b) is a robust feature, but that there is no systematic increase or decrease in the storminess from the present climate to the last glacial maximum one, for either of the storm tracks. Also, simulations from previous studies have not been run according to the same method (e.g., they include the seasonal cycle or not) and therefore do not allow a clear model–model comparison. Most simulations have been run using CLIMAP (1981) reconstructions of sea surface temperatures (SSTs) and ice-sheet elevation. The latter have been suggested to be overestimated (Peltier 1994) and sensitivity studies carried out with the Laboratoire de Météorologie Dynamique (LMD) model show the influence this had on the climate simulations (Ramstein and Joussaume 1995). Our study takes place in the framework of the Palaeoclimate Modelling Intercomparison Project (PMIP) (Joussaume and Taylor 1995), and compares new simulations of the LGM climate all using the CLIMAP SST (if the atmospheric model is not coupled to a slab ocean one), Peltier's ice-sheet reconstructions, and more generally the same changes to boundary conditions. This aids model–model comparisons. In this paper, we examine the simulations run by the European participants to PMIP: the U.K. Universities' Global Atmospheric Modelling Project (UGAMP), Laboratoire des Sciences du Climat et de l'Environnement (LSCE, using the LMD model of Laboratoire de Météorologie Dynamique), U.K. Meteorological Office (UKMO), and the University of Bremen (using the ECHAM3.6 model). The PMIP project, the AGCMs compared, and the methods used to analyze the data are briefly introduced in section 2. A first storm-track comparison of the high-frequency transients is presented in section 3. Section 4 attempts to explain the differences between the storm tracks and to show how these relate to differences in more traditional climate characteristics such as precipitation. Conclusions are drawn in section 5. Our study is restricted to the Northern Hemisphere winter climates for which the storm tracks are best defined

TABLE 1. Some characteristics of the PMIP simulations. The duration of the run does not include the spinup period. The resolution is given via the number of grid points (equivalent gaussian grid in the spectral model cases) of the grid used in the model (in lat, long, and in the vertical, respectively).

	Model	Resolution			Duration (yr)	Type	References
Prescribed SST runs							
ECHAM3	ECHAM3.6	64	128	19	10	spectral	Roeckner et al. (1992)
LSCELMD5H	LMD5.3	72	96	15	15	grid point	Sadourny and Laval (1984)
LSCELMD5	LMD5.3	50	64	11	15	grid point	
LSCELMD4p	LMD4ter	36	48	11	15	grid point	
UGAMP T42p	UGAMP	64	128	19	10	spectral	Dong and Valdes (1995)
UGAMP T21	UGAMP	32	64	19	10	spectral	
Computed SST runs							
LSCELMD4c	LMD4ter	36	48	11	15	grid point	
UGAMP T42c	UGAMP	64	128	19	10	spectral	
UKMO	UKMO3.4	73	96	19	10	grid point	Hewitt and Mitchell (1997)

and the differences between the control and LGM conditions are the largest.

2. The data and its analysis

The PMIP project encourages simulations of the mid-Holocene (6000 yr BP) and LGM (21 000 yr BP) climates using AGCMs forced by the same set of prescribed conditions (hereafter called ''boundary conditions''): the atmospheric composition (in particular CO_2 content), insolation at the top of the atmosphere, land surface conditions, and land–ice distribution for the LGM simulations. Simulations have been run prescribing the sea surface temperatures or computing them by coupling the AGCM to a slab ocean. By comparing the responses from all the models, the project aims to determine the common features of the past climate simulations and help to interpret palaeoclimate data, but also to understand the differences between the model outputs and identify key regions where different behaviors of the models require testing the results against data. The present study clearly lies within the framework of PMIP by focussing on model–model comparison, identifying common changes between the present day and LGM simulations, describing the differences between them, and suggesting reasons for these differences.

The simulations and their main characteristics are given in Table 1 and a summary of the main boundary conditions used to run the models for the present day and LGM simulations is presented in Table 2. The results for the present day climate simulations are compared with the ECMWF reanalyses (ERA) data interpolated on a T42 grid for 10 December–February (DJF) seasons from December 1981 to February 1991, Legates and Willmott (1990) data for the surface temperatures, and Xie and Arkin (1995, 1996, 1997) data for the precipitation.

To describe the storm tracks in the ERA and simulations, high-pass variances have been computed from output taken daily or every 0.75 days.[1] Common available fields included the mean sea level pressure, the geopotential height at 500 hPa, and the zonal and meridional winds at 250 hPa. This led us to compute the mean sea level pressure and 500-hPa geopotential height variance for a first comparison (section 3) and the three-dimensional $\mathbf{E}$ vectors (horizontal $\mathbf{E}$ vectors at 250 hPa and $\overline{v'T'}$ at 700 hPa) for a more detailed study (section 4), the meridional wind and temperature at 700 hPa being available for all but one of the models and giving the possibility to analyze the storm tracks following the method of Hoskins et al. (1983). These diagnostics give an account of the transient activity at different levels and related to different stages of the life of the perturbations for the $\mathbf{E}$ vectors. We concentrate here on the high-frequency variability, that is on perturbations of a timescale lower than 6 days. To single these out, we used Lorenz's ''poor man'' filter described in Hoskins et al. (1989) and used in other studies (Hall et al. 1994, 1996b): high-pass second-order transient eddy quantities are computed according to the formula

$$\overline{x'y'}_{\text{high-pass}} = \frac{1}{N} \sum_{i=1}^{N} x'_i y'_i - \frac{3}{N} \sum_{j=1}^{N/3} x'_{3,j} y'_{3,j},$$

where N is the number of days in the season (in our case), and the subscript 3 denotes averages over consecutive three-day periods. The principle of the filter is that the low-pass variance, computed from averages of the data on consecutive 3-day periods, is subtracted from the total variance. It is similar to a 2–6-day bandpass filter.

---

[1] We do not expect the results to be very sensitive to the frequency of the initial output as calculations from daily and twice-daily data from one of the models did not show significant differences, either in the geographical patterns or in the amplitudes of the computed transients.

TABLE 2. Summary of the boundary conditions for the PMIP runs of the present day and the LGM climates. The changes in CO_2 level can differ according to the model but are calculated so that the radiative forcing changes are the same.

Type of simulation	Present day	Last glacial maximum (LGM)
All	• present insolation	• 21 000 years BP insolation. • Peltier (1994) ice-sheet reconstruction. • CTRL land-surface conditions for snow-free regions. • small changes in land–sea distribution corresponding to a sea level decrease of 105 m.
Prescribed SST	• present SST. • CO_2 = 345 ppm (present value).	• CLIMAP (1981) SST reconstruction. • CO_2 = 200 ppm.
Computed SST	• CO_2 = 280 ppm (pre-industrial value).	• CO_2 = 200 ppm.

3. High-frequency transient eddy diagnostics

Figure 1 shows the high-pass filtered mean sea level pressure variance[2] in the ERA, in all the prescribed SST present day simulations and in the UKMO present day computed SST run. The UGAMP T42c and LSCELMD4c computed SST simulations are fairly similar to their prescribed SST counterparts and are not shown. The two Northern Hemisphere storm tracks appear clearly on the observational analyses and in all the simulations, as maxima of the mean sea level pressure variance off the east coast of the continents. However differences both in the precise position and in the value of the maxima are important. In the ERA, the Pacific storm track is represented by a maximum of more than

---

[2] The variance has been computed for each winter before taking the average over the duration of the run. For convenience, the fields presented here are the square root of this average, whose order of magnitude and units are easier to interpret than the variance's ones.
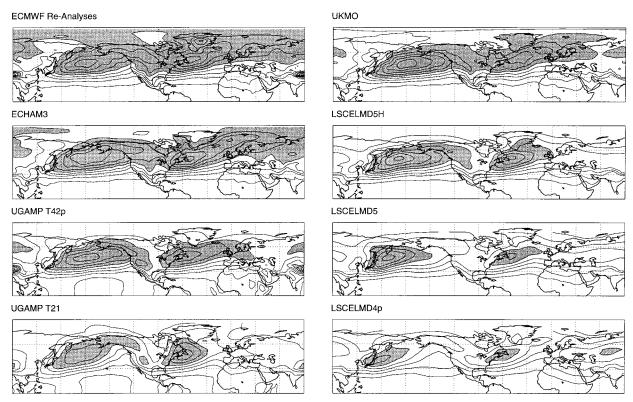

FIG. 1. High-pass mean sea level pressure variance (square root, in hPa) for the DJF season of the present day simulations. Left-hand side, from top to bottom: ECMWF reanalyses, ECHAM, UGAMP T42p, UGAMP T21; right-hand side: UKMO, LSCELMD5H, LSCELMD5, LSCELMD4p. Contours every hPa, shading above 5 hPa.

8 hPa at around (45°N, 180°). The (shaded) region of variances above 5 hPa stretches from the eastern coast of Japan to the interior of the American continent. These features are well reproduced in the UGAMP T42, ECHAM3, LSCELMD5H, and UKMO simulations, with maxima of 8 hPa for the first two and 9 hPa for the last two, but less so in the others: the variance maximum in the LSCELMD5 run is above 8 hPa, but is situated too much to the west (45°N, 160°E) and the corresponding region of high variability does not extend enough to the east. Both the UGAMP T21 and LSCELMD4 runs exhibit weaker maxima (slightly above 6 hPa, well located for the UGAMP T21 run but too much to the west for LSCELMD4) and storm tracks that are too limited in the eastward direction.

The Atlantic storm track reaches its maximum of more than 9 hPa at around (50°N, 50°W) in the ERA, and the shaded region of variances above 5 hPa extends from the American to the European continents. Its structure is more complex than the Pacific one, since from the main core of the storm track situated over New Foundland, there is an extension of the storm track northeastward, over Iceland, and a sharp decrease in the variability east of Iceland compared to the smooth decrease eastward of the maximum of the Pacific storm track. It therefore appears stronger but shorter than the Pacific storm track. In addition, there is a second maximum over eastern Greenland. The main core of the storm track is correctly located in all simulations. As for the Pacific storm track, its magnitude is quite well reproduced in the ECHAM3, UGAMP T42, UKMO, and LSCELMD5H runs, although the value of the maximum in all these simulations, except in the ECHAM3 one, is a little weak (7 or 8 hPa). Even though the main core of the storm track is fairly well represented by these models, the finer structure is not well captured. The high variability over Greenland is absent or only suggested, whereas the northeastward extension of the storm track is generally present but it does not decrease as sharply east of Iceland. ECHAM3 is the only model simulating a strong enough Atlantic storm track compared to the Pacific one, but in this model, the mean sea level pressure variance does not abruptly decrease to the east of Iceland (see, e.g., the 7-hPa contour); its Atlantic storm track is a little too long. For the other runs the main core maximum is generally too weak (7 hPa for UGAMP T21, 6 hPa for LSCELMD5, 5 hPa for LSCELMD4) but correctly located, and as was observed for the Pacific storm track, the length of the region of maximum activity is also restricted in the eastward direction. These storm tracks are generally too weak for the finer structure of the observed storm track to be captured.

A comparison of the 500-hPa geopotential height variances (not shown) confirms that even though all models correctly simulate high variability off the east coast of the continents, the storm tracks are better simulated in their amplitude and longitudinal extension in the higher resolution simulations (ECHAM3, UGAMP T42,

LSCELMD5H, UKMO). However, from this point of view too few models have the stronger Atlantic storm track shown by the ERA. In the end, only ECHAM3 has storm tracks reaching a correct amplitude with the right balance between them.

For the LGM case we first comment on the prescribed SST runs and then the computed SST ones, as the conditions for the development of the extratropical perturbations are different for these two types of simulations. In the first type of experiments the SSTs are set to the CLIMAP dataset in all models. In the second type of runs, they are allowed to vary, within the constraints of prescribed oceanic meridional heat fluxes. The prescribed ocean heat fluxes vary between the models. In all cases, they are chosen so that they well reproduce present day conditions. Over sea ice, the models are free to predict the surface temperature. In addition, the treatment of the ocean heat fluxes under the extensive sea-ice varies between models. The resulting SSTs are shown and further discussed in section 4c but an important fact about them is that they are warmer in the northeastern Atlantic, hence being far less zonal than the CLIMAP distribution in this region.

In all the prescribed SST simulations, both storm tracks significantly shift and/or extend eastward from present day (Fig. 1) to LGM (Fig. 2). The Pacific storm track as described by the mean sea level pressure variance (Fig. 2) shows a larger shift than as described by the 500-hPa geopotential height variance (not shown). On the other hand, the Atlantic storm track undergoes a comparable shift to the east in both diagnostics from present day to LGM simulations, the maxima for the LGM being situated off the European coast, if not over Europe itself for the LSCELMD4, LSCELMD5H, and ECHAM3 runs. Thus, the response to the changes in boundary conditions is shallower over the Pacific than over the Atlantic: for the Pacific storm track, the main difference in the boundary conditions between the LGM and the control is in the SST distribution. Looking more closely to temperature and wind latitude–altitude sections for the western Pacific (not shown) it is evident that the lower half of the troposphere is more perturbed than the upper half, which is relatively unchanged. This will also be seen in the next section in Figs. 6–10. These show how the Atlantic jet stream is much more perturbed at LGM than the Pacific one. Indeed, in the Atlantic case, the presence of the Laurentide ice sheet modifies the flow already affected by changes over the Pacific. The resulting flow, which arrives on a colder Atlantic Ocean, differs from the present day one throughout the troposphere (the differences in SSTs are also larger). Hence, it is not surprising that the changes in transient activity over the Pacific occur more at the surface than at upper levels, while they occur at all levels over the Atlantic.

The computed SST simulations (Fig. 3) show less dramatic changes in the geographical position of the storm tracks from present day to LGM. The Pacific

ECHAM3

LSCELMD5H

UGAMP T42p

LSCELMD5

UGAMP T21

LSCELMD4p

FIG. 2. High-pass mean sea level pressure variance (square root, in hPa) for the DJF season of the last glacial maximum prescribed SST simulations. Left-hand side, from top to bottom: ECHAM, UGAMP T42p, UGAMP T21; right-hand side: LSCELMD5H, LSCELMD5, LSCELMD4p. Contours every hPa, shading above 5 hPa.
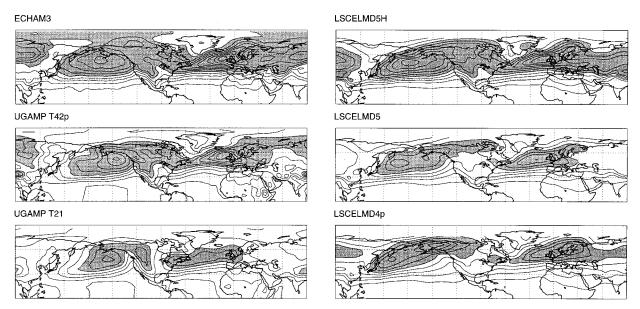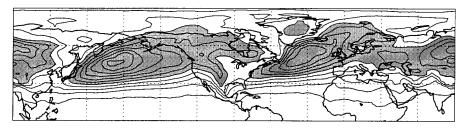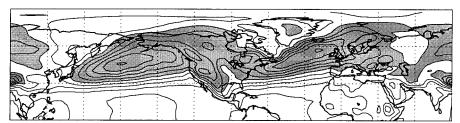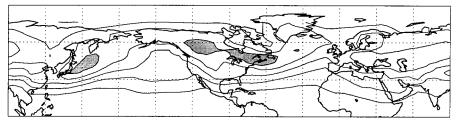
UKMO

UGAMP T42c

LSCELMD4c

FIG. 3. High-pass mean sea level pressure variance (square root, in hPa) for the DJF season of the last glacial maximum computed SST simulations. From top to bottom: UKMO, UGAMPT42c, LMD4terc. Contours every hPa, shading above 5 hPa.
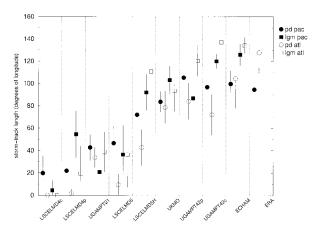
Fig. 4. Length of the 65-m contour of the high-pass 500-hPa geopotential variance. The largest extension is considered to be of 150° long for both storm tracks. The errors bars given are for ± one standard deviation around the mean value. Circle: present day storm tracks, squares: LGM storm tracks; black symbol: Pacific storm track, white symbol: Atlantic storm track.

storm track does not move significantly but, as in the prescribed SST simulations, the Atlantic storm track shows a significant shift to the east at all levels (geopotential height variance at 500 hPa not shown), except in the LSCELMD4 simulations where variances are weak and quite stable. Nevertheless this shift is not as large as in the prescribed SST case. Hence, the differences in the position of the storm tracks between present day and LGM simulations are more important in the prescribed SST simulations than in the computed SST ones. For the two models for which there is a computed and a prescribed SST run, the difference between those is more significant at LGM than at present day. These differences are detailed in Dong and Valdes (1998) for the UGAMP model, and will be discussed in section 4c.

Figure 4 summarizes the previous results by giving the average length of each storm track for each simulation. The longitudinal extension of the storm track has been retrieved for each DJF season by looking for the grid boxes where the high-frequency 500-hPa geopotential variance was higher than 65 m in the 30°–60°N, 105°E–105°W region for the Pacific storm track and in the 30°–70°N, 105°W–45°E region for the Atlantic storm track. Therefore, the mean but also the standard deviation of these results are presented, giving an indication of the variability of the storm tracks, which could not be shown on the previous figures. Figure 4 confirms that the higher resolution models' Pacific storm tracks lie within the range of the ERA, whereas for the Atlantic storm track, only the ECHAM model approaches the ERA results. For all the simulations, there is a clear separation between the lower (LSCELMD4, LSCELMD5, UGAMP T21) and higher (LSCELMD5H, UKMO, UGAMP T42, ECHAM3) resolution models, with significantly shorter storm tracks in the former ones. All models except LSCELMD4c show an increase in the Atlantic storm track from the present day to the

LGM, which appears quite robust, while the changes in the Pacific storm-track length seem less so, although the higher resolution models consistently give an increase of the storm track, except UGAMP T42p.

For both diagnostics discussed here, the differences in the storm tracks simulated in the present day runs are confirmed by the LGM ones. They seem to be mainly linked to the resolution of the models, as was suggested in previous studies (Boville 1991; Rind 1988; Senior 1995) and as is evident from the comparison of the UGAMP T42 and T21 runs and the LSCELMD5H and LSCELMD5 ones. However, resolution is not the only factor explaining the differences in the storm-track representation, which is proved by the differences between the UGAMP T42 and the ECHAM3 T42 simulations, and between the LSCELMD5 and UKMO runs, which are nevertheless smaller than between models of different resolutions. What cannot be seen from Fig. 4 is the position of the storm track and its changes from present day to LGM simulations. Nearly all models give an eastward shift for both storm tracks, more marked for the Atlantic one. The two different diagnostics discussed here show consistent changes from present day to LGM, although these changes can be different at the surface and at 500 hPa, as exemplified by the Pacific storm-track case in the prescribed SST simulations. We can also note here that while the present day Atlantic storm-track maximum is (correctly) situated at the same location for all models, this position fluctuates for all other cases. The mechanism responsible for this feature must be different for the particular case of the present day Atlantic storm track. In the next section, the study of the three-dimensional **E** vectors allows us to diagnose the storm tracks at different stages of their life cycle and at their corresponding levels and to describe them in a more precise way. We also examine the relationship betweem the storm tracks, the mean flow, and the surface climatological characteristics.

4. Differences between the storm tracks: Reasons and implications

In this section, we examine more closely the relationship between the storm tracks and the baroclinicity of the simulated mean general circulation, as described by the meridional gradients in surface temperatures and the vertical shear of the zonal mean flow. We then show how the characteristics of the precipitation patterns are linked to those of the storm tracks and associated stationary waves. After introducing observed results for the present climate, we concentrate on three points: the mechanisms responsible for the differences between models of different resolutions (UGAMP and LSCELMD runs) in section 4a; the differences due to the representation of the physics in two models using the same representation of the dynamics, at the same resolution (UGAMP and ECHAM3) in section 4b; the differences due to the computation of the SSTs (com-

puted SST runs of the UGAMP, LMD, and UKMO models) in section 4c.

To describe the storm tracks we use the three-dimensional $\mathbf{E}$ vector of Hoskins et al. (1983) defined as follows in pressure coordinates:

$$\mathbf{E}_{3D} = (\overline{v'^2 - u'^2}, \; -\overline{u'v'}, \; -f_0\overline{v'\theta'}/\Theta_p),$$

where u and v are the zonal and meridional components of the velocity, f_0 the Coriolis parameter, θ the potential temperature, and Θ_p the vertical gradient of the potential temperature profile in pressure coordinates.

As suggested in Hoskins et al. (1983), $\mathbf{E}_{3D}$ is plotted in the following way: its vertical component is represented by $\overline{v'T'}$ at 700 hPa; it is representative of the activity of the perturbations at their early, growing stage. Then its zonal and meridional components are represented in a vector form at 250 hPa, where in principle they reach their maximum; they correspond to the activity of the perturbations at their mature stage, when it has reached the upper levels of the troposphere. Hence, in addition to being a description of the storm tracks as were the mean sea level pressure and 500-hPa geopotential height variances, the $\mathbf{E}$ vectors allow us to follow the activity of the perturbations at their early and mature stages. Moreover the divergence of the $\mathbf{E}$ vectors gives an account of the influence of the eddies on the mean flow: divergent (convergent) $\mathbf{E}$ vectors mean that the eddies exert a westerly (easterly) forcing on the mean flow. Therefore it gives more complete information about the storm tracks than the diagnostics presented in section 3 but could not be used for this first comparison as it was not available for all models.

In the Northern Hemisphere midlatitudes, the observed surface temperatures [from Legates and Willmott (1990), Fig. 5a] show their sharpest gradients off the east coast of the continents. Accordingly, the zonal wind at 250 hPa (from ERA) reaches its maxima over these regions, with a maximum slightly stronger for the Pacific jet than for the Atlantic one (over the Pacific, the zonal wind is also forced by the stationary waves due to orography and tropical heating, but in the present study we focus more on the changes in baroclinicity implied by the changes in SSTs). The stationary waves associated with the variations of the jet stream can be seen through the 850-hPa winds (Fig. 5b), which show troughs over the western part of the oceans and ridges above the continents. The Pacific storm track (from ERA, Fig. 5c) develops in the oceanic trough at the exit of the Pacific jet, with a maximum of 20 km s^{-1} in the 700-hPa high-pass eddy temperature flux. The horizontal components of the high-pass 250-hPa $\mathbf{E}$ vectors peak downstream of the $\overline{v'T'}$ maximum, above the eastern Pacific. Most of the precipitation pattern [from Xie and Arkin (1995, 1996, 1997), Fig. 5e] over the midlatitude Pacific, is clearly associable with the storm track. The maxima above the west coast of America appear to be also linked to the mean advection over the high orography of warm and moist air by the southwesterlies of the end of the storm track (Fig. 5b).

According to the $\mathbf{E}$ vectors, the upper-level eddy activity is also high above the American continent, the region that includes the end of the Pacific storm track but also the region of frequent cyclogeneses in the lee of the Rockies. This influences the Atlantic storm track, which is characterized by a high-pass 700-hPa eddy temperature flux maximum of more than 20 K m s^{-1} at around (50°N, 50°W) and by $\mathbf{E}$ vectors peaking slightly downstream of this $\overline{v'T'}$ maximum. It essentially differs from the Pacific one because the $\mathbf{E}$ vectors are already quite strong at its western end. The divergence of the $\mathbf{E}$ vectors (Fig. 5d) shows that the mean flow undergoes a westerly acceleration in the lee of the Rockies and off the American east coast under the effect of the high-frequency transient eddies. The forcing by the total transient eddies (not shown) follows a similar pattern, with, in addition, a region of easterly acceleration over eastern America. This forcing is very different from the Pacific one, which is weakly easterly at the beginning of the storm track and strongly westerly at its end (in the high-pass filtered and total components). The influence of the eddies on the mean flow only appears in association with the storm track over the Pacific, and is not significant in the western part of the jet stream over Asia. On the other hand, the eddy forcing on the Atlantic jet stream over America appears much more important. In both cases, the high-frequency eddies help maintain the jet stream since in the eastern part of the storm track, the eddy forcing is westerly. This influence is modulated by the low-frequency eddy forcing, which is easterly over the central Atlantic, but the total forcing remains westerly over the Atlantic midlatitudes. It is also modulated by the third component of the $\mathbf{E}$ vectors, that is, the meridional heat fluxes, which are likely to be convergent in the western part of the regions of strong $\mathbf{E}$ vectors over the oceans, but which are probably less significant over the continents and at the end of the storm tracks. The $\mathbf{E}$ vectors and their divergence therefore show that the transient eddies play a different role in the Pacific and the Atlantic storm tracks. Over the Pacific they appear to help maintain baroclinic conditions in the eastern part of the storm track, whereas over the Atlantic they also appear to have an important role in forcing the jet stream at the beginning of the storm track.

All diagnostics, including those from section 3 (Fig. 1), show that the Atlantic storm track is stronger than the Pacific one. The precipitation is equally stronger, reaching its maximum of around 8 mm day^{-1} in the region of high $\overline{v'T'}$ and $\mathbf{E}$ vectors. One may note that the storm track and precipitation over the Atlantic are stronger than over the Pacific whereas the jet stream and baroclinicity are actually weaker on the Atlantic. This is likely to be related to the different seasonality of the two Northern Hemisphere storm tracks: while the Atlantic storm track peaks in winter and is at its lowest

surface temperatures and 250 hPa winds   Legates and Willmott and ERA

(a)

850 hPa winds - 10 m/s   →   ERA

(b)

3D E-vectors - 100 m²/s²   →   ERA

(c)

250 hPa E-vector divergence   ERA

(d)
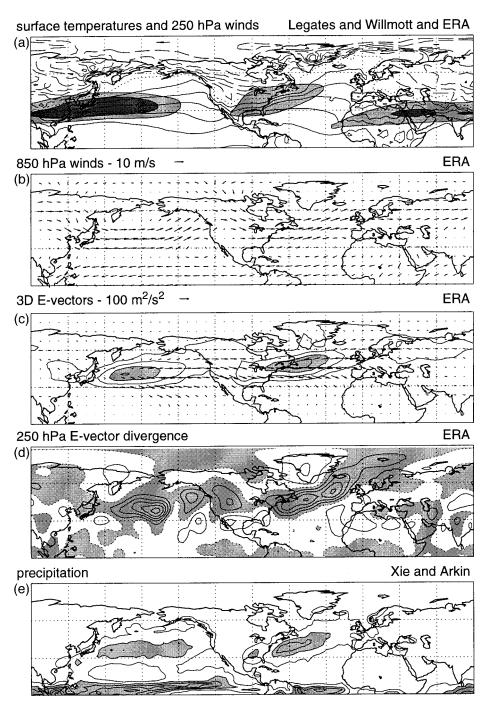
precipitation   Xie and Arkin

(e)

FIG. 5. Results from observations [surface temperatures from Legates and Willmott (1990) and precipitation from Xie and Arkin (1995, 1996, 1997)] and ECMWF reanalyses for the DJF season. From top to bottom: (a) surface temperatures, contours every 5°C, 0°C contour dotted, negative contours dashed, and 250-hPa zonal wind, 30 m s^{-1} and 45 m s^{-1} contours, light shading between 30 and 45 m s^{-1} darker shading above 45 m s^{-1}. (b) The 850-hPa horizontal wind, unit arrow corresponding to 10 m s^{-1}. (c) High-pass eddy temperature flux at 700 hPa, contours every 5 K m s^{-1}, shading for values above 15 K m s^{-1}, and 250-hPa **E** vectors, unit arrow corresponding to 100 m² s^{-2}. (d) 250-hPa high-pass filtered horizontal **E** vector divergence, contours every 2×10^{-5} m s^{-2}, shading for positive values. The field has been slightly smoothed for clarity. (e) Precipitation rate, contours for 2, 4, 6, 8, and 10 mm day^{-1}, shading above 4 mm day^{-1}.
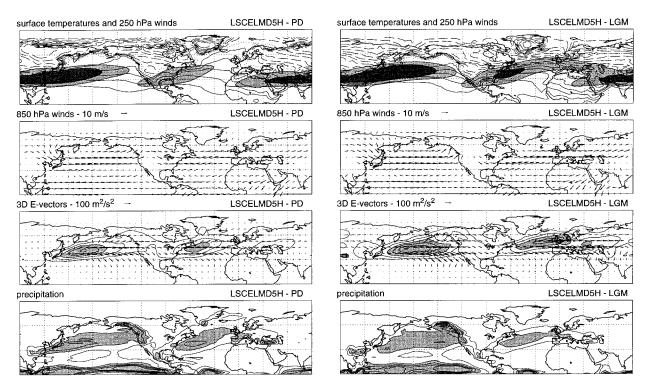
FIG. 6. Same results as in Fig. 5 (plotted with the same conventions) but for the LSCELMD5H simulations of the present day climate (left-hand side) and LGM one (right-hand side). The **E** vector divergence has been omitted.

in summer, the Pacific storm track reaches its maxima in the equinoctial seasons and shows a local minimum in winter. This may be due to the perturbations being advected by the very strong mean-flow before they develop as fully as in autumn or spring (Nakamura 1992). This phenomenon is not observed for the Atlantic storm track because the jet is weaker.

a. Sensitivity to resolution

The simulations compared here provide us with two opportunities to investigate the models' sensitivity to resolution. The UGAMP model has been run with prescribed SSTs at resolutions of T21 and T42, with only the parameterizations linked to resolution (such as the horizontal diffusion) being modified between the two runs; the LSCELMD5 and LSCELMD5H simulations have been produced by the same model, LMD version 5.3, at resolutions of $50 \times 64 \times 11$ (number of grid points regularly spaced in sine of the latitude, in longitude and irregularly distributed in the vertical) and $72 \times 96 \times 15$, respectively. In addition, the LSCELMD4 runs have been produced with a previous version of the same model: LMD4ter, at a lower resolution: $36 \times 48 \times 11$. The main parameterization changes between the LMD4ter and LMD5.3 versions of the model concern surface parameterizations such as snow albedo, sea ice, vegetation and drag coefficients [cf. Masson and Joussaume (1997); Masson et al. (1998)].

In section 3 we noticed the improvement towards the ERA of the storm tracks in the LSCELMD4, LSCELMD5, and LSCELMD5H simulations on the one hand, and of the UGAMP T21 and T42 on the other. To understand this, we first look at the mean-flow and surface characteristics of the LSCELMD runs on the left-hand side top pictures of Figs. 6, 7, and 8 for the present day climate simulations (to be compared to observations and ERA Fig. 5). LSCELMD4 (Fig. 8) shows significant discrepancies compared to the ERA: the Pacific jet stream's exit (first left-hand side plot) is situated very much to the west and a secondary, unrealistic maximum forms off the Californian coast and extends throughout the American continent into a weak Atlantic jet. The low-level winds (second left-hand side plot) are not realistic either, with southwesterlies over the central part of the oceans, west of the ERA southwesterlies, which lie over the east of the oceans. In the LSCELMD5 run (Fig. 7), the Pacific jet stream is better represented, and the Atlantic one is well positioned over the American east coast but is too weak. Furthermore, the low-level stationary waves are correctly simulated. The LSCELMD5H run (Fig. 6) shows jet streams and low-level winds very similar to the analysis ones, and, in particular, a stronger Atlantic jet stream than in the LSCELMD5 run. The improvement with resolution of the representation of the mean-flow characteristics is thus very obvious from these three LSCELMD runs, as

surface temperatures and 250 hPa winds   LSCELMD5 - PD

surface temperatures and 250 hPa winds   LSCELMD5 - LGM

850 hPa winds - 10 m/s →   LSCELMD5 - PD

850 hPa winds - 10 m/s →   LSCELMD5 - LGM

3D E-vectors - 100 m²/s² →   LSCELMD5 - PD

3D E-vectors - 100 m²/s² →   LSCELMD5 - LGM

precipitation   LSCELMD5 - PD

precipitation   LSCELMD5 - LGM

FIG. 7. Same results as in Fig. 6 (plotted with the same conventions) but for the LSCELMD5 simulations of the present day climate (left-hand side) and LGM one (right-hand side).

surface temperatures and 250 hPa winds   LSCELMD4 - PD

surface temperatures and 250 hPa winds   LSCELMD4 - LGM

850 hPa winds - 10 m/s →   LSCELMD4 - PD

850 hPa winds - 10 m/s →   LSCELMD4 - LGM

3D E-vectors - 50 m²/s² →   LSCELMD4 - PD

3D E-vectors - 50 m²/s² →   LSCELMD4 - LGM

precipitation   LSCELMD4 - PD

precipitation   LSCELMD4 - LGM

FIG. 8. Same results as in Fig. 6 (plotted with the same conventions, except for the **E** vectors) but for the LSCELMD4p simulations of the present day climate (left-hand side) and LGM one (right-hand side).

surface temperatures and 250 hPa winds UGAMP T42 - PD

surface temperatures and 250 hPa winds UGAMP T42 - LGM

850 hPa winds - 10 m/s → UGAMP T42 - PD

850 hPa winds - 10 m/s → UGAMP T42 - LGM

3D E-vectors - 100 m²/s² → UGAMP T42 - PD

3D E-vectors - 100 m²/s² → UGAMP T42 - LGM

250 hPa E-vector divergence UGAMP T42 - PD

250 hPa E-vector divergence UGAMP T42 - LGM

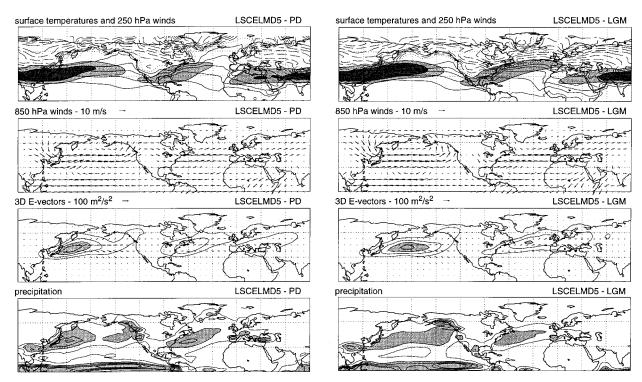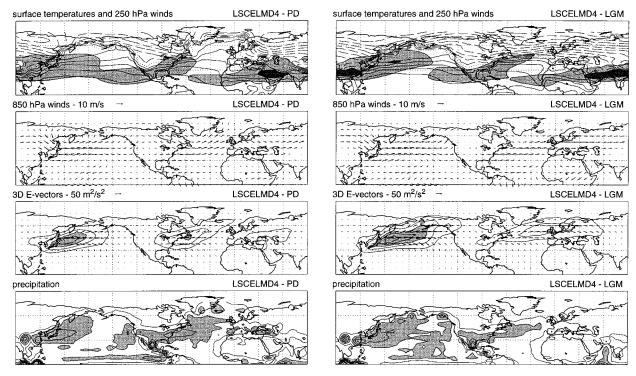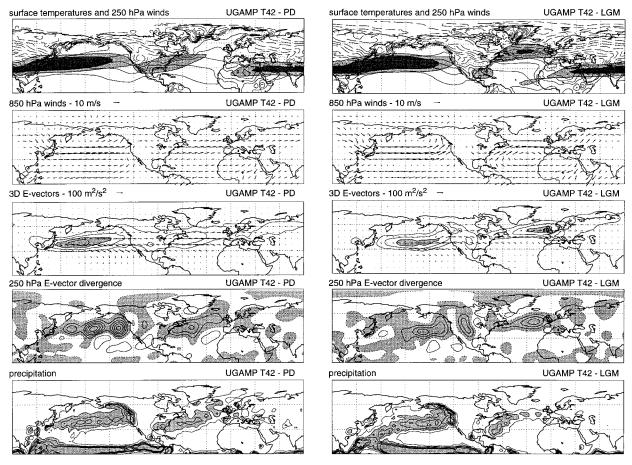precipitation UGAMP T42 - PD

precipitation UGAMP T42 - LGM

FIG. 9. Same results as in Fig. 5 (plotted with the same conventions) but for the UGAMP T42p simulations of the present day climate (left-hand side) and LGM one (right-hand side).

well as in the UGAMP runs (Fig. 9 for the UGAMP T42 run, UGAMP T21 omitted).

It is also remarkable in the transient diagnostics. The Pacific storm track's region of high 700-hPa eddy temperature flux is well captured in all the runs. The main difference between the models is at upper levels where the strength and location of the 250-hPa horizontal **E** vectors improve with resolution: in the LSCELMD4 run, they are small and confined to the western Pacific right above the region of high $\overline{v'T'}$; in the LSCELMD5 one, they move downstream from this region; in LSCELMD5H, they get stronger. The same behavior is observed in the UGAMP runs. Hence, in all the runs the eddy activity is correctly generated at low levels but is not well represented downstream and at higher levels at low resolutions. Only the highest resolution LSCELMD5H and UGAMP T42 give evidence of significant eddy activity over the eastern Pacific and the American continent; it appears negligible in the low resolution simulations. Thus, thinking in terms of the divergence of the **E** vectors (not shown), we can relate the shortness of the Pacific jet stream in the low-resolution simulations to the weakness of the **E** vectors over

the central and eastern Pacific, which implies a weaker (or easterly, in some cases) influence of the eddies on the mean-flow and therefore a weaker jet stream there. Also, the secondary maximum in zonal wind in the LSCELMD4 simulation off the American west coast seems to be forced by low-frequency eddies (not shown), which clearly shows the influence the eddies can have on the mean flow. Given the small **E** vectors over America in the low resolution runs, one can infer that the eddy forcing on the mean flow there is not well captured. Even in the higher resolution LSCELMD5 and UGAMP T42 runs, although the pattern of the forcing is well represented, its amplitude is too weak (see Fig. 9 for the UGAMP case). This has an influence on the Atlantic storm track, which representation improves with resolution as it is the case for the Pacific storm track, but does not reach the amplitude of the ERA, even in the higher resolution runs. Hence, for the Atlantic storm track, in addition to the features noticed for the Pacific one, there is also the problem of representing well the eddies and their influence on the mean flow at the beginning of the storm track.

Thus the small longitudinal extension of the storm

tracks in the low resolution runs (seen in Fig. 4) can be explained slightly differently for the Pacific and Atlantic storm tracks. The perturbations appear to form adequately over the Pacific but not to be well represented at the nonlinear stage of their development; on the other hand, over the Atlantic, the conditions at the beginning of the storm track, and, in particular, the weakness of the eddies and of their influence on the mean flow over America, account for less eddy activity from the start and then, as for the Pacific, the perturbations do not develop realistically. In the higher resolution UGAMP T42 and LSCELMD5H runs, the propagation of the eddy activity upward and downstream is represented better. However, for the Atlantic storm track, the interaction between transient eddies and mean flow appears to be too weak in both simulations, and the LSCELMD5H storm track might be stronger than the UGAMP T42 one only because this model tends to develop stronger eddies for the same background conditions, as seems to be the case for the Pacific storm track.

The improvements in the simulated precipitation with resolution are not as striking as those in the atmospheric circulation but for each of the models the regions of high precipitation, which are confined to the east of the oceans in the low resolution runs, extend eastward with increasing resolution. Moreover the precipitation on the American west coast is not well represented in low resolution runs such as LSCELMD4, in which both the storm track and the southwesterlies are not well modeled over this region. Most models overestimate the Pacific precipitation and underestimate the Atlantic one, which can be related to the weakness of the Atlantic storm track compared to the Pacific one.

The characteristics of the present day simulations described above are also found in the LGM simulations (right-hand side of Figs. 6, 7, 8, and 9). However, consistently in all LGM simulations, the Pacific storm track moves eastward together with the exit of the stronger baroclinic zone. This has a consequence on the precipitation patterns, which also move and/or extend eastward. The Atlantic storm track is dragged eastward by the zone of high baroclinicity situated across the Atlantic over the sea-ice edge and is therefore farther away from the Pacific storm track. Note that changes (especially in the jet stream) are larger over the Atlantic than over the Pacific, as introduced in the previous section. In the low resolution models, there is no evidence of upper-level eddy activity over America, while both LSCELMD5H and UGAMP T42 give some. However, the Atlantic storm track appears to develop quite independently from the transient eddies above the American continent and their forcing on the mean flow. Rather, its location, which is the same for LSCELMD5H and UGAMP T42, seems to be determined by the surface temperature gradients associated with the presence of the sea-ice edge over the midlatitude Atlantic, whereas its strength does seem to be linked to the eddy activity and its divergence upstream, but for the LGM the key region is the western Atlantic. In the LSCELMD5H run, the **E** vectors divergence over the west Atlantic is stronger than in the UGAMP T42 run, which can explain the stronger jet stream and storm track. At the end of the storm track, over Europe, the LSCELMD5H **E** vector divergence is also stronger than the UGAMP T42 one and this can be linked to the longitude of the southwesterlies associated with the end of the storm track, which is more to the east in the LSCELMD5H run.

On the Atlantic, in all the runs, the presence of sea ice explains the significant decrease in precipitation. The low level mean circulation appears to play a role not only in the Pacific in the higher resolution runs as in the present day simulations, but also on the west Atlantic where maxima in precipitation can be associated not with maxima in storminess, but rather with the mean advection of moist air by southwesterlies that could be forced by the prescribed SSTs (this phenomenon is not so strong in the computed SST experiments).

Hence, resolution appears to have a strong influence on the simulated climates. Because the perturbations cannot develop correctly in the low resolution runs, the storminess is too weak at the eastern end of the storm tracks and so is the precipitation. This weakness of the storm tracks is also related, via an incorrect eddy forcing, to different planetary waves, implying low-level southwesterlies at the end of the storm tracks and maxima of the jet stream at different locations and, hence, a different baroclinicity, particularly over the Atlantic. The eddy activity and its related forcing also plays a role in the higher resolution runs, in which the Atlantic storm track's strength (but not necessarily location) appears to be dependent on the eddy activity over America in the present day case, and over the west Atlantic in the LGM case.

b. Comparison between two T42 models: UGAMP and ECHAM3

Having examined the influence of resolution on the climate simulations in the previous section, we now compare two models run at the same spectral resolution of T42: UGAMP (Fig. 9) and ECHAM3 (Fig. 10). The basic equations have been discretized in the same way for both models, so that they differ only through their sets of parameterizations. The Pacific storm track simulated by the ECHAM3 model for the present climate (Fig. 10) is very similar to the UGAMP one (Fig. 9), as seen from the mean sea level pressure variance in section 3 or through the 700-hPa eddy temperature flux. On the other hand, all these diagnostics show a stronger Atlantic storm track in the ECHAM3 simulation, resulting in a more realistic balance between the two storm tracks, but these differences are always smaller than the ones observed previously between models of very different resolutions.

The two present day Pacific storm tracks, although similar at their initial stage, differ once the eddy activity
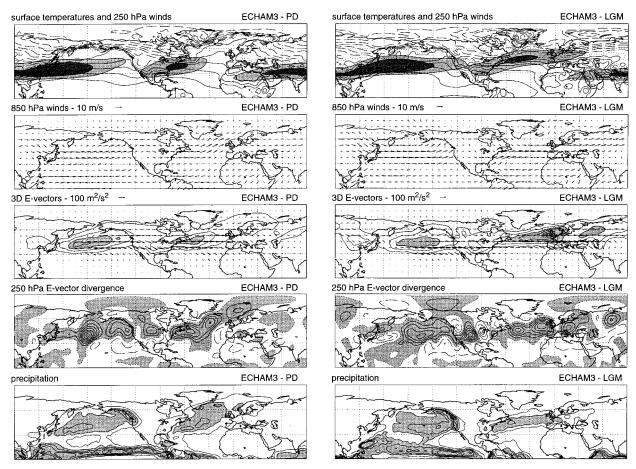
FIG. 10. Same results as in Fig. 5 (plotted with the same conventions) but for the ECHAM3 simulations of the present day climate (left-hand side) and LGM one (right-hand side).

reaches upper levels: the 250-hPa **E** vectors are much stronger in the ECHAM3 run over the Pacific. Over the American continent, the **E** vectors and their divergence are stronger than in the UGAMP T42 run, which can be linked to a stronger Atlantic jet stream and storm tracks. Also, at the end of the storm track, the westerly acceleration of the mean flow under the influence of the high-frequency transient eddies is stronger in the ECHAM3 run. The values of this forcing are too strong to the east of Iceland compared to the ERA, which is consistent with the storm track being too long (cf. Fig. 1). On the other hand, the forcing is weak over the east Atlantic in the UGAMP run, which correlates with its shorter storm track. The ECHAM3 storm tracks give lower and more realistic precipitation and the improvement in the modeling of the Atlantic storm track shows in the better balance in the Atlantic and Pacific precipitation, although it is still a little weak over the Atlantic.

The changes from present day to LGM simulations for the Pacific storm track are very similar for both the ECHAM3 and the UGAMP models (Figs. 9 and 10, right-hand side): the higher temperature gradients over most of the Pacific relate to a stronger jet stream whose

exit is situated more to the east. The storm track shifts eastward following the jet exit and decreases slightly. The same patterns can be recognized in the changes in precipitation, with a shift of the main core of precipitation over the central and eastern Pacific and an increase over the American west coast linked with the more southerly circulation.

Over the Atlantic, the differences between the models are much larger than for the present day simulations. The upper-level changes are also much larger than over the Pacific, showing that the response is less shallow over the Atlantic, as was discussed in section 3. First, the eddy activity over America is still an important feature in the ECHAM3 run south of the Laurentide ice sheet, while it is weak in the UGAMP one. The divergence of the **E** vectors actually indicates that the influence of the eddies on the mean flow is larger in the UGAMP T42 LGM run than in the present day one, but it is still smaller than in the ECHAM3 run. Furthermore, it is much weaker over the western Atlantic in the UGAMP run, which can be associated with a weaker jet stream over the sea-ice edge. This confirms the conclusions from the comparison between the UGAMP T42

and LSCELMD5H in the previous section. The larger baroclinicity in the ECHAM3 run can be linked to much stronger eddy temperature fluxes and **E** vectors that show a very strong transient activity, even over central Europe. The precipitation is also higher over the eastern Atlantic, Europe, and on the south of the Fennoscandian ice sheet, showing that the changes in storm tracks are dominating over the effect of the generally colder air. Over Europe, at the end of the Atlantic storm track, the **E** vector divergence patterns are also different, and as was noticed when comparing the LSCELMD5H and UGAMP T42 simulations, this can be related to the position of the mean southwesterlies of the end of the storm track.

The ECHAM3 and UGAMP T42 models are the only ones with the same resolution and discretization of the basic equations in the set of models studied here, which makes their comparison particularly interesting. The precipitation is generally weaker in the ECHAM3 model, revealing differences in cloud and precipitation parameterizations. The precipitation patterns in the ECHAM3 present day run show evidence of the better representation of the storm tracks in this model. In particular, the forcing of the Atlantic jet stream by the transient eddies over America appears as a key factor for its correct modeling. In the LGM case, this forcing still appears to be important to explain the strength of the Atlantic storm track, in addition to the eddy forcing over the west Atlantic. These explain the large strengthening of the ECHAM3 Atlantic storm track, compared to the weak UGAMP one, which leads to stronger precipitation over Europe and potentially to a different source term in the ice-sheet mass balance budget.

This difference in the eddy activity at upper levels at the end of the storm tracks could be due to the different parameterizations of the horizontal diffusion in the two models. Indeed the approach used in this parameterization in the two models is different (Phillips 1994; Roeckner et al. 1992). To evaluate the impact of the different types of parameterization, we ran the UGAMP model for 3 yr, replacing its horizontal diffusion schemes by the ECHAM3 one. The results show a better balance of the two storm tracks but they both become weaker and are not comparable, in their amplitude, to the ECHAM3 ones. Other differences in the models' parameterizations, such as the vertical diffusion and convection, are therefore playing an important part in explaining the differences in the transient activity they simulate. The representation of orography (mean orography in the ECHAM3 model, enhanced orography in the UGAMP model) might also be responsible for some of the difference, especially as far as the eddy activity over America is concerned.

c. Computed SST simulations

In the previous sections we saw the importance of the SST distribution in driving the changes in storm tracks from present day to last glacial maximum. In this context, computed SST simulations are of interest, since in these runs the sea surface temperatures are not prescribed as one of the boundary conditions, but calculated from a slab ocean model, in which the meridional transport of energy (or q flux) is prescribed. For all the computed SST simulations presented in this paper, including the LGM ones, this meridional flux is computed from a control prescribed SST run. For the LGM simulations, the oceanic meridional fluxes of ocean grid points that become land grid points (due to the sea level decrease) are redistributed homogeneously over the remaining ocean grid points at the same latitude. Note that the assumption behind all these simulations is that the q fluxes (and, hence, the ocean heat transport) do not change between the present and LGM. Hence, all the simulations have been run with the same method, but the so-called q-flux corrections are specific to each model. Allowing the SSTs and sea-ice extent to vary is an important change to the simulations. The differences are small for the present day runs (since the oceanic meridional heat fluxes are held constant and are based on present day prescribed SST runs) but large in the LGM runs, which are forced by the same fluxes.

For two models (LSCELMD4 and UGAMP T42) both types of simulations have been run and the present day computed SST simulations (not shown) are very similar to their prescribed SST counterparts (see section 4a). In addition, as seen in section 3, the UKMO present day simulation (Fig. 11) compares generally well with the observations. Over the Pacific the computed sea surface temperatures are close to the observed ones while the upper-level jet is a little strong. Unfortunately, the 700-hPa eddy temperature flux is not available for these simulations so that it is not possible to estimate the transient activity corresponding to the early development of perturbations in the model. At upper levels the **E** vectors become significant at the same latitude as in the analyses and are actually stronger over the eastern Pacific and over the American continent. As in most models, the precipitation is a little overestimated compared to the climatotology from the Xie and Arkin (1995, 1996, 1997) data, but the pattern is realistic. The results are overall very similar to the LSCELMD5H run of the same resolution. Over the Atlantic, the simulated jet and storm track are a little weak compared to LSCELMD5H and ERA and weaker than the Pacific storm track, as in most models. The precipitation is also weaker than over the Pacific, which makes it very realistic. The weak Atlantic storm track seems to be related to the region of strong temperature gradients off the American east coast not extending enough to the east and to the upper-level eddy activity not being high enough at the beginning of the storm track, over the American east coast. More precisely, this low in the **E** vector amplitude implies a convergence/divergence pattern over and off the east of America, respectively, which is much stronger than in the ERA, from which we can infer a different forcing from the eddies on the mean flow.

surface temperatures and 250 hPa winds UKMO - PD

surface temperatures and 250 hPa winds UKMO - LGM

850 hPa winds - 10 m/s → UKMO - PD

850 hPa winds - 10 m/s → UKMO - LGM

3D E-vectors - 100 m²/s² → UKMO - PD

3D E-vectors - 100 m²/s² → UKMO - LGM

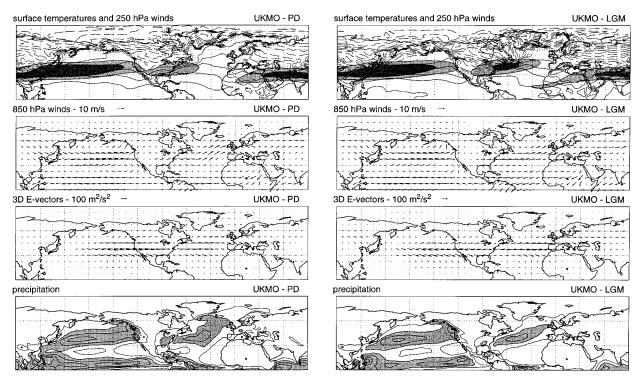precipitation UKMO - PD

precipitation UKMO - LGM

FIG. 11. Same results as in Fig. 6 (plotted with the same conventions) but for the UKMO simulations of the present day climate (left-hand side) and LGM one (right-hand side). The eddy temperature flux at 700 hPa is not available.

surface temperatures and 250 hPa winds UGAMP T42c - LGM

surface temperatures and 250 hPa winds LSCELMD4c - LGM

850 hPa winds - 10 m/s → UGAMP T42c - LGM

850 hPa winds - 10 m/s → LSCELMD4c - LGM

3D E-vectors - 100 m²/s² → UGAMP T42c - LGM

3D E-vectors - 50 m²/s² → LSCELMD4c - LGM

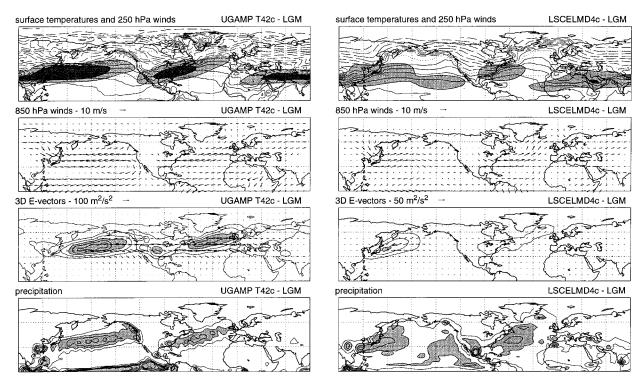precipitation UGAMP T42c - LGM

precipitation LSCELMD4c - LGM

FIG. 12. Same results as in Fig. 6 (plotted with the same conventions, except for the LSCELMD4c **E** vectors) but for the UGAMP T42c LGM simulation (left-hand side) and the LSCELMD4c LGM simulation (right-hand side).

Contrary to the present day situation, the LGM computed SST simulations (Fig. 12 for the UGAMP and LSCELMD4 results, and Fig. 11 for the UKMO simulation) contrast significantly with the prescribed SST ones. The computed SSTs differ from the prescribed CLIMAP ones: they are still quite similar over the Pacific except for the UGAMP model, which gives an important cooling of the surface and sea-ice formation in the northwestern Pacific, while all three models give a warmer eastern Atlantic. Differences between the computed and CLIMAP SSTs are due to the prescribed meridional oceanic heat fluxes taken from the control runs and/or to the feedback from the atmosphere. Differences between the computed SSTs themselves on the other hand are likely to be due to differences in the treatment of the q fluxes for ice-covered oceans.

Over the Pacific, the changes from the present day to the LGM simulations in the UKMO and LSCELMD4 runs are not very important compared to the ones in the prescribed SST simulations. In particular the storm track does not move as much eastward. Consistently the precipitation patterns do not change much either. On the other hand, the UGAMP extensive sea ice relates to tighter SST gradients and to a stronger storm track but the precipitation decreases due to the storm track being partly situated over the sea ice. Over the Atlantic, even if the SSTs are warmer than the CLIMAP distribution, the changes are important and consistent with the changes found with the prescribed SST simulations. Both high resolution runs (UGAMP T42c and UKMO) show a strengthening of the upper-level jet stream over the west Atlantic and of the storm track, which moves eastward. The precipitation does not change as much as the storm track but one has to take into account the fact that the air is much colder at LGM than at present. It is stronger than in the prescribed SST experiments, especially over the eastern ice-free part of the ocean, showing that the stability in precipitation from present day to the LGM in the computed SST runs is probably a manifestation of a stronger storm track.

In the two cases in which we have both prescribed and computed SST simulations (UGAMP T42 and LSCELMD4), at LGM (Figs. 8 and 9, right-hand side, to be compared to Fig. 12), there is a reorganization of the storm tracks and stationary waves. The latter apparently carry more energy in the LSCELMD4 computed SST run to the detriment of the storm tracks, while the opposite is happening in the UGAMP T42 computed SST run. Indeed, if we compare the contributions of the zonally averaged meridional transport $[\overline{vT}]$ at 700 hPa due to the stationary eddies and to the transient eddies in each of the LGM runs, we find that in the UGAMP T42 prescribed SST simulation, the contribution due to the stationary eddies reaches 20 K m s^{-1} and the one due to the total transient eddies 11 K m s^{-1}; in the UGAMP T42 computed SST run, the stationary eddy contribution peaks at 15 K m s^{-1}, and the transient eddy one at 17 K m s^{-1}. On the other hand, in LSCELMD4p, the stationary eddy contribution's maximum is 9 K m

s^{-1} compared to the transient eddy contribution: 17 K m s^{-1}; in LSCELMD4c, the stationary eddy contribution's maximum increases to 11 K m s^{-1}, while the transient eddy one decreases to 14 K m s^{-1}. This reorganization of the stationary waves is particularly obvious above the Atlantic where the winds are southwesterly in the LSCELMD4 computed SST run instead of more westerly in the prescribed SST one, whereas the circulation follows the American east coast and then is constrained by the long sea-ice edge in the UGAMP T42 prescribed SST run instead of the smoother and more zonal one in the computed SST experiment. In the latter run, the storm tracks are much stronger, especially the Atlantic one, related to stronger baroclinicity and eddy forcing, following mechanisms similar to those seen in the ECHAM3 simulation in the previous section.

The LGM experiments show the differences created by the computation of SSTs. These appear to influence the storm track and the precipitation, which is particularly sensitive to the position of the storm track with respect to the sea-ice edge. Despite these differences between the two types of runs examined here, the changes simulated for LGM are not contradictory. In particular, applying the same reasoning as for the prescribed SST runs, we can explain the differences in the storm tracks, and, especially over the Atlantic, the changes are consistent. However it is difficult to generalize results from computed SST runs as we have only three of them at our disposition.

5. Conclusions

These simulations, run in the framework of the PMIP project using the same conditions, allow a close comparison of the models not only in their ability to reproduce the present day climate, but also a radically different one: the last glacial maximum climate. From the 10 sets of simulations for the present day and last glacial maximum climates discussed in this paper, we can deduce the general mechanisms that explain the differences between the two climates as simulated and forced by different boundary conditions: at the last glacial maximum, the surface temperature in the Tropics is the same or slightly higher than at present day, whereas the temperature in the northern high latitudes is much lower due to the presence of the ice sheets. This cold temperature also implies the formation of sea ice more to the south than in the present day. This is particularly dramatic over the Atlantic, and forces tight temperature gradients around the sea-ice edge. It is therefore not surprising to see, in the CLIMAP dataset and in the surface temperatures computed by the models in the computed SST runs, increased baroclinicity in the traditional baroclinic zones off the eastern coasts of the continents and across the Atlantic Ocean along the sea-ice edge. A common feature forced by this increased baroclinicity is the eastward shift of both storm tracks. The Pacific storm track moves eastward following the exit of the zone of high temperature gradients and of

the jet stream, whereas the Atlantic one is driven eastward by the tight temperature gradients associated with the sea-ice edge. These changes in the storm tracks are linked to changes in the stationary waves, in particular, the flow is more zonal over the Atlantic due to the nearly zonal ice-edge there, and those two effects combined have an impact on the precipitation patterns. These have to be interpreted keeping in mind that the LGM climate is cooler and thus less favorable to precipitation. Changes in storm tracks over the oceans and in the southerlies or southwesterlies in the stationary waves, in particular off the coasts of America are generally correlated with similar but less spectacular changes in precipitation if the storm track is not located over the sea ice. If they are, the precipitation is smaller due to the atmosphere above the sea ice being much cooler and the sea ice cutting the moisture and energy heat fluxes from the ocean to the atmosphere.

These changes take place in all the simulations. However, there are large differences, most of which can be related to differences in the present day simulations. The largest difference in the storm-track representation is associated with the resolution of the models and confirms what had already been noticed by Boville (1991), Rind (1988), and Senior (1995). The higher the resolution, the better the storm tracks are modeled. What we clearly show here, using appropriate diagnostics such as **E** vectors, is that the eddy activity at low levels (as seen by the 700-hPa eddy temperature fluxes), is not as resolution-dependent as the upper-level transients, which are associated with the mature and nonlinear stage of the perturbations' life cycle. In the low resolution models, in the present day simulations, the transient eddy activity over the Pacific is generally well generated at low levels but does not develop correctly toward its mature and decaying stages, upward and downstream. The same applies to the Atlantic storm track, which, in addition, appears to be well modeled only when the transient eddies and their forcing over America are well represented, which is delicate even in the higher resolution models. Hence, in the low resolution present day runs, the Atlantic storm track is weak not only because the nonlinear development of the perturbation is not correctly modeled, but also because the inital conditions for this development are poorly represented. At this point it has to be noted that most of the previous AGCM studies of the LGM climate have been run at resolutions lower or comparable to the lowest resolutions present in this study. Their results concerning the storminess and precipitation patterns at midlatitudes therefore have to be analyzed taking into account the implications of this low resolution.

As for the changes from present day to LGM, it is noticeable that a higher baroclinicity off the eastern coasts of the continents does not necessarily imply stronger transients, as Nakamura (1992) noted for the present day observed Pacific storm track. Indeed, the decrease of the storm track with an increasing jet stream is seen in some of the simulations, particularly over the Pacific. In fact, the models react differently to the change in baroclinicity: the heat transport from equator to pole is reorganized in various ways, giving more or less importance to the transients on the one hand, and to the stationary waves on the other. Obviously the latter are of major importance in the low resolution models in which the day-to-day variability is weak.

The Atlantic storm track appears to develop more independently of the conditions over North America at LGM when the extensive sea-ice edge across the Atlantic ocean pulls the storm track significantly eastward. This can explain the fact that in this case, as for the present day and LGM Pacific storm tracks, the Atlantic storm-track maxima are not located at the same position for all models. This contrasts with the present day Atlantic storm track, whose position is more determined by land–sea contrasts and is the same for all models. Even though the Atlantic LGM storm track is located farther eastward, the higher resolution models show that the influence of the transient eddies and their feedback on the mean flow over America and off the American east coast should not get underestimated. In particular, the ECHAM3 and LSCELMD5H high resolution models have a very strong Atlantic storm track at LGM, much stronger than in any of the other models, which seems to be related to the feedback from the transient eddies over the west Atlantic, rather than over the American continent. Indeed, cyclogenesis over America is certainly affected by the changes of orography due to the presence of the Laurentide ice sheet. Studying the differences between the ECHAM3 and UGAMP T42 simulations gives an idea of the differences attributable to the different parameterizations in the models, which have the same resolution and use the same discretization of the basic equations. This example shows that the simulated last glacial maximum climate is dependent not only on the boundary conditions imposed to the model but also on the interactions within the atmosphere, for example, the influence of the eddy activity over America on the Atlantic storm track. This mechanism is negligible in the lower-resolution models due to the limited eastward extension of the storm tracks, and this should be kept in mind when analyzing them.

The computed SST simulations show the dependence of the simulated climate on the SSTs. In these runs, these are not prescribed from the CLIMAP dataset but computed from prescribed oceanic heat fluxes, coming from control simulations from the same model. Hence, the simulated LGM climate is not necessarily very realistic but gives us the chance to see the changes in storminess and precipitation under different surface conditions. In all the computed SST experiments, the Pacific storm track is not as different from the present day one as in the prescribed SST runs. On the other hand, the SSTs computed on the Atlantic are much warmer on its eastern part, which makes the temperature gradients along the sea-ice edge much less zonal, and the storm tracks and precipitation stronger, at least in the higher resolution models.

The simulated climate at the last glacial maximum is most sensitive to the model at the eastern end of the storm tracks, and particularly over Europe and the Fennoscandian ice sheet since the strength of the Atlantic storm track depends not only on its correct simulation but also on a correct simulation of the transient eddies over America. This is most important when establishing the ice-sheet mass balance budget, since those are situated in the areas where the model results are most different. The west coasts of the continents are therefore regions where it would be particularly useful to check the models against paleodata. Also, although the data to quantify this factor is not available, one can imagine that the surface drag over the oceans are quite different in the LGM simulations and between the models, which has important implications for the oceanic circulation.

REFERENCES

Blackmon, M. L., 1976: A climatological spectral study of the 500-mb geopotential height of the Northern Hemisphere. *J. Atmos. Sci.,* **33,** 1607–1623.

——, J. M. Wallace, N.-C. Lau, and S. J. Mullen, 1977: An observational study of the Northern Hemisphere wintertime circulation. *J. Atmos. Sci.,* **34,** 1040–1053.

——, Y.-H. Lee, and J. M. Wallace, 1984: Horizontal structure of 500-mb height fluctuations with long, intermediate and short timescales. *J. Atmos. Sci.,* **41,** 961–979.

Boville, B. A., 1991: Sensitivity of simulated climate to model resolution. *J. Climate,* **4,** 469–485.

Charney, J. G., 1947: The dynamics of long waves in a baroclinic westerly current. *J. Meteor.,* **4,** 135–163.

CLIMAP, 1981: Seasonal reconstructions of the earth's surface at the Last Glacial Maximum. Geophysical Society of America Map Chart Series MC-36, 1–18.

Dong, B., and P. J. Valdes, 1995: Sensitivity studies of Northern Hemisphere glaciation using an atmospheric general circulation model. *J. Climate,* **8,** 2471–2496.

——, and ——, 1998: Simulations of the Last Glacial Maximum climates using a general circulation model: Prescribed versus computed sea surface temperatures. *Climate Dyn.,* **14,** 571–591.

Eady, E. T., 1949: Long waves and cyclone waves. *Tellus,* **1,** 33–52.

Hall, N. M. J., B. J. Hoskins, P. J. Valdes, and C. A. Senior, 1994: Storm tracks in a high-resolution GCM with doubled carbon dioxide. *Quart. J. Roy. Meteor. Soc.,* **120,** 1209–1230.

——, B. Dong, and P. J. Valdes, 1996a: Atmospheric equilibrium, instability and energy transport at the last glacial maximum. *Climate Dyn.,* **12,** 497–511.

——, ——, and ——, 1996b: The maintenance of the last great ice sheets: A UGAMP GCM study. *J. Climate,* **9,** 1004–1019.

Hewitt, C. D., and J. F. B. Mitchell, 1997: Radiative forcing and response of a GCM to ice age boundary conditions: Cloud feedback and climate sensitivity. *Climate Dyn.,* **13,** 821–834.

Hoskins, B. J., and P. J. Valdes, 1990: On the existence of storm-tracks. *J. Atmos. Sci.,* **47,** 1854–1864.

——, I. N. James, and G. H. White, 1983: The shape, propagation and mean-flow interaction of large-scale weather systems. *J. Atmos. Sci.,* **40,** 1595–1612.

——, H. H. Hsu, I. N. James, M. Masutani, P. D. Sardeshmukh, and G. H. White, 1989: Diagnostics of the global atmospheric circulation based on ECMWF analyses 1979–1989. WRCP Tech. Rep. 27, 217 pp.

Joussaume, S., and K. Taylor, 1995: Status of the Paleoclimate Modeling Intercomparison Project (PMIP). *Proc. First International AMIP Scientific Conference,* Monterey, CA, WRCP, 425–430.

Kutzbach, J. E., and P. J. Guetter, 1986: The influence of changing orbital parameters and surface boundary conditions on climate simulations for the past 18 000 years. *J. Atmos. Sci.,* **43,** 1726–1759.

Legates, D. R., and C. J. Willmott, 1990: Mean seasonal and spatial variability in gauge-corrected, global precipitation. *Int. J. Climatol.,* **10,** 111–127.

Lim, G. H., and J. M. Wallace, 1991: Structure and evolution of baroclinic waves as inferred from regression analysis. *J. Atmos. Sci.,* **48,** 1718–1732.

Masson, V., and S. Joussaume, 1997: Energetics of the 6000-yr BP atmospheric circulation in boreal summer, from large-scale to monsoon areas: A study with two versions of the LMD AGCM. *J. Climate,* **10,** 2888–2903.

——, ——, S. Pinot, and G. Ramstein, 1998: Impact of parameterizations on simulated winter mid-Holocene and Last Glacial Maximum climatic changes in the Northern Hemisphere. *J. Geophys. Res.,* **103,** 8935–8946.

Nakamura, H., 1992: Midwinter suppression of baroclinic wave activity in the Pacific. *J. Atmos. Sci.,* **49,** 1629–1642.

Peltier, W. R., 1994: Ice age paleotopography. *Science,* **265,** 195–201.

Phillips, T. J., 1994: A summary documentation of the AMIP models. PCMDI Tech. Rep. 18, 343 pp. [Available from National Technical Information Service, U.S. Department of Commerce, 5285 Port Royal Rd., Springfield, VA 22161.]

Ramstein, G., and S. Joussaume, 1995: Sensitivity experiments to sea surface temperatures, sea-ice extent and ice-sheet reconstruction, for the last glacial maximum. *Ann. Glaciol.,* **21,** 343–347.

Rind, D., 1987: Components of the ice age circulation. *J. Geophys. Res.,* **92,** 4241–4281.

——, 1988: Dependence of warm and cold climate depiction on climate model resolution. *J. Climate,* **1,** 965–997.

Roeckner, E., and Coauthors, 1992: Simulation of the present-day climate with the ECHAM model: Impact of the model physics and resolution. Max-Planck-Institut für Meteorologie Tech. Rep. 93, 171 pp. [Available from Max-Planck-Institut für Meteorologie, Bundesstrasse 55, D-20146 Hamburg, Germany.]

Sadourny, R., and K. Laval, 1984: January and July performance of the LMD general circulation model. *New Perspectives in Climate Modelling,* A. Berger and C. Nicolis, Eds., Developments in Atmospheric Science, Vol. 16, Elsevier, 173–198.

Senior, C. A., 1995: The dependence of climate sensitivity on the horizontal resolution of a GCM. *J. Climate,* **8,** 2860–2880.

Simmons, A. J., and B. J. Hoskins, 1980: Barotropic influences on the growth and decay of nonlinear baroclinic waves. *J. Atmos. Sci.,* **37,** 1679–1684.

Thorncroft, C. D., B. J. Hoskins, and M. E. McIntyre, 1993: Two paradigms of baroclinic-wave life-cycle behaviour. *Quart. J. Roy. Meteor. Soc.,* **119,** 17–55.

Wallace, J. M., G.-H. Lim, and M. L. Blackmon, 1988: Relationship between cyclone tracks, anticyclone tracks and baroclinic waveguides. *J. Atmos. Sci.,* **45,** 439–463.

Xie, P., and P. A. Arkin, 1995: An intercomparison of gauge observations and satellite estimates of monthly precipitation. *J. Appl. Meteor.,* **34,** 1143–1160.

——, and ——, 1996: Analyses of global monthly precipitation using gauge observations, satellite estimates, and numerical model predictions. *J. Climate,* **9,** 840–858.

——, and ——, 1997: Global precipitation: A 17-year monthly analysis based on gauge observations, satellite estimates, and numerical model outputs. *Bull. Amer. Meteor. Soc.,* **78,** 2539–2558.